



Nixon-Pearson, O. J., & Hallett, S. R. (2015). An investigation into the damage development and residual strengths of open-hole specimens in fatigue. *Composites Part A: Applied Science and Manufacturing*, 69, 266-278. [10.1016/j.compositesa.2014.11.013](https://doi.org/10.1016/j.compositesa.2014.11.013)

Peer reviewed version

Link to published version (if available):  
[10.1016/j.compositesa.2014.11.013](https://doi.org/10.1016/j.compositesa.2014.11.013)

[Link to publication record in Explore Bristol Research](#)  
PDF-document

## University of Bristol - Explore Bristol Research

### General rights

This document is made available in accordance with publisher policies. Please cite only the published version using the reference above. Full terms of use are available:  
<http://www.bristol.ac.uk/pure/about/ebr-terms.html>

### Take down policy

Explore Bristol Research is a digital archive and the intention is that deposited content should not be removed. However, if you believe that this version of the work breaches copyright law please contact [open-access@bristol.ac.uk](mailto:open-access@bristol.ac.uk) and include the following information in your message:

- Your contact details
- Bibliographic details for the item, including a URL
- An outline of the nature of the complaint

On receipt of your message the Open Access Team will immediately investigate your claim, make an initial judgement of the validity of the claim and, where appropriate, withdraw the item in question from public view.

## **An investigation into the damage development and residual strengths of open-hole specimens in fatigue.**

O. J. Nixon-Pearson<sup>a\*</sup>, and S.R. Hallett<sup>a</sup>

*a - Advanced Composites Centre for Innovation and Science,  
University of Bristol, Queen's Building, University Walk, Bristol BS8 1TR, UK*

*\* Corresponding author, Email: on5405@bristol.ac.uk, Tel: +44 (0)117 3315797*

### **Abstract**

An extensive experimental program was carried out to investigate and understand the sequence of damage development throughout the life of open-hole composite laminates loaded in tension-tension fatigue. Quasi-isotropic carbon/epoxy laminates, with stacking sequence  $[45_2/90_2/-45_2/0_2]_S$ ,  $[45/90/-45/0]_{2S}$  and  $[45/90/-45/0]_{4S}$  were examined. These were selected on the basis that under quasi-static loading the  $[45_2/90_2/-45_2/0_2]_S$  configuration exhibited a delamination dominated mode of failure whilst the  $[45/90/-45/0]_{2S}$  and  $[45/90/-45/0]_{4S}$  configurations showed a fibre dominated failure mode, previously described as “pull-out” and “brittle” respectively. Specimens were fatigue loaded to  $1 \times 10^6$  cycles or catastrophic failure, whichever occurred first. A number of tests were interrupted at various points as the stiffness dropped with increasing cycles, which were inspected using X-ray Computed Tomography (CT) scanning. A static residual strength program was carried out for run-out specimens of each configuration.

**Keywords:** *A. Carbon-fibre; B. Fatigue; B. Fracture; X-ray Computed Tomography.*

### **Introduction**

Fibre-reinforced composites laminates are increasingly being used to manufacture load bearing primary structures in the aerospace industry as composites offer a much greater strength to weight ratio than metals. The initial perception was that composite materials don't suffer from the effects of fatigue, however in recent years it has become well established that composites can exhibit damage under cyclic loading conditions. Laminates with stress concentrations have complex damage sequences and failure events, and show a wide variety of effects not observed in un-notched laminates. The notch sensitivity of a laminate in terms of mechanical

properties, depends on various factors, such as: laminate thickness, ply orientations, laminate size, notch size, and machining quality. These factors all affect the way damage propagates, their interactions and the final mode of failure. In previous work, Spearing and Beaumont [1] concentrated on tension-tension fatigue of notched Carbon/Epoxy (T300/914) and Carbon/Polyetheretherketone (PEEK) laminates using an R ratio of 0.1. NDT (non-destructive testing) techniques included X-radiography to produce images of the damage. It was also shown how prolonged exposure to the zinc iodide dye penetrant can accelerate the growth of damage in the specimens.

Broughton et. al. [2] have investigated open-hole tension-tension fatigue behaviour of a quasi-isotropic glass-fibre reinforced plastic GFRP laminate under constant amplitude and block amplitude loading. They showed that longitudinal strain, stiffness and surface temperature can be used to assess damage progression and fatigue life, and are potentially suitable for predicting notched fatigue performance. They also showed how the application of various measurement techniques such as fibre-Bragg grating (FBG) and digital image correlation (DIC) can be useful for fatigue damage assessment, and also highlighted localised sub-critical damage at the hole edge.

Kawai and Shiratsuchi [3] studied the effects of centrally located circular holes on the constant amplitude fatigue behaviour of cross-ply CFRP laminates of various stacking sequences. They showed how the notched fatigue strength of cross ply laminates becomes lower than for un-notched specimens in the range of short fatigue life. However for the long life range this notch sensitivity becomes insignificant. So a new method for prediction of fatigue strengths of composites was developed with the assumption that notch sensitivity reduces during fatigue loading.

Early work carried out by Mohlin et. al [4, 5] using tetrabromoethane (TBE) enhanced X-ray radiography involved the study of delamination growth in notched/carbon epoxy laminates under compressive fatigue loading. They used the prepreg system T300/1034E with a stacking sequence  $[\pm 45/0_2/\pm 45/90/0_3/\pm 45/0_2]_S$  and an R ratio of  $-\infty$  with a frequency of between 6 and 10 Hz. An R ratio of  $-\infty$  implies that the loading is in compression with a maximum amplitude of zero. At intervals during the fatigue test, the specimens were X-

rayed using TBE as the dye penetrant. The specimens were placed onto a film and X-rayed using an energy of 60 kV and 200 mA with an exposure time of 0.45 seconds. At all load amplitudes from 48-88% of the static fracture compressive load, matrix cracks in the 0° ply orientations (along the direction of loading) occurred tangential to the hole edges below  $10^3$  cycles. After further cycling, delaminations began to propagate outwards between the interfaces of the off axis plies until catastrophic failure occurs.

The main limitations of this early work is the 2D nature of damage characterisation, and the inability to separate out the global damage into individual delamination interfaces and ply cracking orientations. Fatigue damage in composites is distinctly three dimensional in character and therefore more recent techniques such as X-ray computed tomography (CT) are much more suitable for the evaluation of the micromechanical behaviour of fatigue damage development. More recently, as high resolution X-ray computed tomography (CT) has become available as an experimental technique. Work by Scott et. al. [6] and Moffat et. al.[7] had proven the capability of this technique to identify damage progression in notched carbon-epoxy specimens under quasi-static loading to failure.

Fatigue damage accumulation at the vicinity of the hole causes a redistribution of stresses giving rise to the notch blunting effect observed in the literature. This results in an increase in the residual strength post-fatigue, over untested specimens. However, matrix cracking, fibre breakages and delaminations deteriorate mechanical properties such as stiffness and weaken the composite laminate. Bakis, Simmonds and Stinchcombe [8-11], carried out a systematic study on the effects of stacking sequence, matrix type, and stress ratio on residual strength. They found that for each composite material, a critical cyclic stress level exists where the residual strengths begin to decrease below that of the untested specimens.

Other work, by Ambu et. al. [12] investigated the residual properties of composites after undergoing fatigue. They carried out a study on the effects of damage on the residual strength of open-hole laminates subjected to fatigue. They found that DIC proved to be very useful tool in order to clarify the roles played by various failure modes on the residual properties of open-hole laminates. However this technique isn't useful for predicting with

accuracy the stiffness loss of the laminate to failure due to damage initiating mostly at the surface plies, thereby rendering further strain measurements inaccurate.

It is important to clarify that for unidirectional laminated composites, the extent of splitting in the load bearing  $0^\circ$  plies is responsible for the reduction of the stress concentrations around a notch tip giving enhanced failure strengths post-fatigue. Spearing and Beaumont [13] have showed that this is the case for  $[90/0]_S$  centre-notched cross ply specimens, where the laminate only fails when the strength of a ligament between the  $0^\circ$  ply splits is exceeded by the stress concentration localised at the notch tip.

Wang and Shin [14] also observed notch blunting effects in open-hole composite laminates. They based their study on  $[0/90]_{4S}$  AS4/PEEK thermoplastic laminates which could be reconsolidated to remove all damage apart from fibre breakages. Despite this the reconsolidated specimens revealed no change in the strength from the unconsolidated specimen. TBE enhanced X-radiography showed that the  $0^\circ$  ply splits grew significantly during the first 500,000 cycles but remained fairly constant up to  $10^6$  cycles. As PEEK has a much greater toughness compared with thermoset resins, there was comparably little delamination and matrix cracking allowing the damage to develop in the form of  $0^\circ$  splits tangential to the hole.

For matrix dominated failure in notched composites such as those described as delamination failures in [15], this mechanism no longer exists since final specimen failure is due to the progression of matrix damage, usually starting at the hole-edge rather than the effect of the stress concentration on the fibres. Thus increased post-fatigue strengths caused by notch blunting are not observed, however this is not well clarified in the open literature.

To date many of the studies in the literature have concentrated on the macro-scopic effects of fatigue damage on mechanical properties and there have been few studies into the detailed damage mechanisms and sequence of events occurring, such as in [16-19]. There has also been a large amount of work describing various residual strength models and their fit to experimental data. However there has been little work carried out on the development of fatigue damage at the micro-scale using X-ray CT, especially on the characterisation and understanding of the damage prior to residual strength tests using different layups and specimen geometries.

This paper describes, compares and characterises the fatigue damage events in open-hole tensile tests using X-ray CT on various different quasi-isotropic configurations of unidirectional carbon/epoxy prepreg and their effects on residual strength.

## 2. Experimental Procedure

The material used is a carbon fibre-epoxy unidirectional (UD) prepreg system, IM7/8552, manufactured by Hexcel. The material was chosen as it is widely used within the aerospace sector. The UD prepreg tapes have a nominal ply thickness of 0.125 mm. The properties are available from the manufacturer's data sheet [20].

The laminates were autoclave cured using Hexcel's recommended cure cycle [20].

The specimen comprises of a parallel edge gauge section of constant cross sectional area  $A$ , width  $w$ , thickness  $t$ , and a gauge length of 64mm for all cases. At each end of the specimen gauge section are the gripping areas.

The specimen had a central hole-diameter,  $d$ , and a constant ratio of  $w/d=5$  for each of the configurations. Holes were drilled using lip and spur, tungsten carbide drill bits. The ratio of width to hole diameter was chosen as it represent the minimum distance needed to allow the elastic stress states to return sufficiently close to their original values at the edges, thereby giving dimensions offering the lowest failure forces, whilst using the least amount of material.

The general stacking sequence is  $[+45_m/90_m/-45_m/0_m]_{ns}$ , which has the load bearing plies in the 0 direction away from the surface and they are thus more protected from impact damage, which is consistent with standard industry practice. From previous quasi-static work [15] there are two methods of scaling the thickness. The first is by using ply-level scaling, which is defined as blocking together plies of the same orientation where  $n=1$  and  $m$  is any integer, the second, is sub-laminate-level scaling where the basic stacking sequence of sub-laminates  $[+45/90/-45/0]_s$  is repeated where  $m=1$  and  $n$  is any integer.

Previous work on quasi-static loading of open-hole tension tests showed three distinct failure modes, characterised as delamination, pull-out and brittle [15]. In this paper each of these three failure mechanisms are investigated under fatigue loading, using the smallest specimen configuration which gave the required failure mode under quasi-static loading. For delamination failure this is the ply-level scaled laminate with  $m=2$  and  $n=1$

with a central hole of 3.175 mm. The same thickness sub-laminate-level layup with  $m=1$ ,  $n=2$ , and  $d=3.175\text{mm}$  gave a pull-out failure (referred to in this paper as the baseline sub-laminate case), For brittle failure all the dimensions of the sub-laminate layup needed to be increased by a factor of 2 from the baseline to give a second sub-laminate configuration with  $m=1$ ,  $n=4$ , and  $d=6.35\text{mm}$ . In this study the gauge length for this configuration was reduced by half from [15] to 64mm in order to save on material costs since it was shown from the static tests that damage was localised around the hole and did not propagate extensively along the gauge length. Table 1 below shows each of three specimen configurations of interest:

**Table 1 Showing the dimensions for each configuration to be tested [15].**

Hole Diameter, d (mm(inch))	Width, w (mm)	Thickness, t (mm)	Layup	Quasi-static Failure mode [15]
3.175 (1/8)	16	2	$m=2$ , $n=1$	Delamination
3.175 (1/8)	16	2	$m=1$ , $n=2$	Pull-out
6.35 (1/4)	32	4	$m=1$ , $n=4$	Brittle

Each of the failure mechanisms are determined by the amount of subcritical damage which occurs prior to final failure. Under fatigue loading it is expected that there will be differences in this subcritical damage growth and thus variations in final failure. Quasi-statically, pull-out failure occurs when the fibre failure stresses of the  $0^\circ$  plies are reached during full width delamination of the surface  $45/90$  and  $-45/0$  interfaces. This partial delamination allows some plies to “pull out” from between each other at the point of fibre failure. If the fibre failure stress has not been reached at the point by which the delamination at the  $-45/0$  interface is fully developed across the width then delamination failure back to the specimen grips occurs. Brittle failure occurs with little or no delamination present. Failure occurs across the full width of the specimen with clean fracture surfaces through the entire laminate with the fracture plane normal to both hole edges and perpendicular to the direction of loading, breaking fibres in every orientation.

A small number of quasi-static tests (minimum three per configuration) were repeated to allow for different material batches from [15]. For these tests, the specimens were loaded at 1mm/min in the  $0^\circ$  direction until failure. A mean static failure load could then be established. The fatigue tests were run with peak amplitudes at various percentages of the (average) static failure load, this is what is commonly defined as severity in the literature. Fatigue specimens were then loaded in tension-tension fatigue with  $R=0.1$  at 5Hz at various amplitudes to  $1 \times 10^6$  cycles or catastrophic failure (defined as a 15% drop in stiffness), which ever occurred first.

To characterise the effect of damage propagating under fatigue from the hole and free edge a stiffness,  $E'$ , is calculated by using  $E' = FL/\delta A = F/\epsilon A$ , where  $F$  is the force at maximum amplitude,  $A$  as the gross cross sectional area of the specimens and  $\epsilon$  is the strain measured using a clip gauge extensometer recorded over a gauge length of 50 mm symmetric about the hole for each specimen.

The ply-level case has been previously reported in [19]. There are a total of 5 severities (or load levels) were used, 6 specimens were tested at 80% severity, 10 were tested at 70%, 11 at 60% (excludes interrupted tests which did not satisfy the failure criterion), 6 at 50%, and 8 at 40% (run-outs). For the baseline sub-laminate case, 7 severities were used, 4 specimens were tested at 90%, 6 at 85%, 5 at 80%, 5 at 70%, 2 at 60%, 5 at 65%, and 5 at 55%. A number of tests were interrupted at various points as the stiffness dropped with increasing cycles, using 60% severity tests in the ply-level case and 80% severity tests in the baseline sub-laminate case in order to accurately determine a sequence of damage events leading to catastrophic failure in fatigue. Fatigue tests were terminated at  $1 \times 10^6$  cycles if no failure occurred. This is termed as a run-out. For load levels that reached  $1 \times 10^6$  cycles, three further specimens were tested to run-out in order to ascertain that the fatigue life exceeded  $1 \times 10^6$  cycles. Each run-out specimen was tested for post-fatigue residual strength. A second sub-laminate configuration was tested, 3 specimens were fatigue tested each at 90% and 85% severity, and a single specimen at 75% severity. All specimens tested using this configuration went to a run-out. Tests were carried out for post-fatigue residual strength using three specimens each for 90% and 85% severity run-outs.

## **2.1 3D X – ray Computed Tomography**

Acoustic emission, optical microscopy, scanning electron microscopy and ultrasonic C –scan have all previously been exploited to characterise damage development. However acoustic emission and C-scan have limited resolution and can be ambiguous in terms of identifying the damage mechanism; optical and electron microscopy are surface methods as is DIC and so cannot provide a 3D analysis of the system. Consequently, X-ray CT is rapidly becoming an increasingly important tool in the micromechanical damage analysis of materials [21] enabling routine non-destructive 3D imaging in the micron range. This technique was thus chosen for extensive damage characterisation of the specimens tested in this experimental programme.



In order to describe the initial pre-fatigue damage in specimens, several quasi static tests were interrupted at 60%, 70% and 80% of the nominal failure load for ply-level specimens and 70%, 80%, and 85%, nominal failure load for the baseline sub-laminate case. An interrupted test was also carried out for the second sub-laminate case at 90% as there is very limited information on the subcritical damage of this configuration in [22]. Selected fatigue tests for the ply-level and sub-laminate level tests were also interrupted at various stages of damage accumulation, as indicated by the decrease in effective modulus.

Interrupted test specimens from quasi-static, and fatigue loading along with run-out specimens were inspected using X-ray Computed Tomography (CT) scanning in order to determine the level of damage in each specimen. CT reconstructions were carried out on each sample after scanning. This enables visualisation of a given sample as a 3D map in which features of interest such as delaminations and matrix cracking could be identified. To enhance X-ray contrast these samples were soaked in X-ray dye penetrant comprising of 250g zinc iodide, 80ml distilled water, 80ml isopropyl alcohol and 1ml kodak photoflo®, over a period of 2 days. Zinc iodide was used because it is relatively non-toxic and is reasonably X-ray opaque.

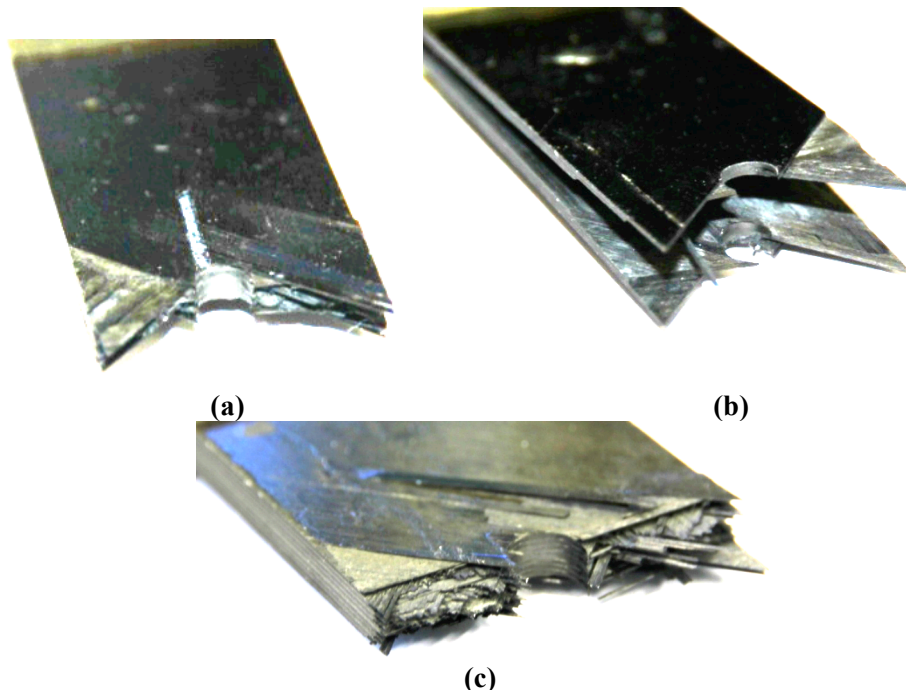
Micro X-ray CT was performed at the National Composites Centre (NCC) using a Nikon X-Tek 320kV electron beam machine. Each specimen is mounted on the rotation stage and positioned between the X-ray source and the 16 bit 2000x2000 pixel panel detector. A cone of X-rays are emitted from the target and pass through the specimen to the detector. During the scan, the specimen is incrementally rotated through 360° about the longitudinal axis of the specimen, with a radiograph (projection) collected at each orientation. The individual set of radiographs projections are reconstructed into a 3D volume using a filtered back-projection reconstruction algorithm. The scanning voltage was 80kV (with 150 $\mu$ A) and the exposure time for each radiograph was 250 milliseconds. The Metris CT Pro software was used to reconstruct each scan volume with manipulation and analysis performed using VG Studio Max 2.1 and Avizo® 7 software packages. This enables visualisation of the volumes of a given sample as a 3D map in which the grey scale value corresponds to the local X-ray absorption coefficient of the material. There are two peaks on the histogram of the grey scale intensity which indicate the solid material (fibres and matrix), and air (matrix cracking, delaminations, voids and other defects). Hence the

matrix cracks and delaminations could be segmented by defining certain thresholds around the appropriated grey scale values [23]. See [6] and [19] for further details on segmentation.

### 3. Quasi-static Testing

Specimens of each layup were loaded to failure using a displacement rate of 1mm/min. Failure was taken as the first significant drop on the load-displacement curve (>5%). Previous quasi-static tests using various thicknesses and layups had shown the three distinct failure modes [15] described in section 2.

The tests in this present study represent a configuration from each of the pull-out and brittle failure modes as well as a recap of the delamination case already presented in [19]. In all cases quasi-static tests were repeated before commencing the fatigue testing programme. Due to the large number of specimens used in the fatigue testing programme, made over a period of time, a number of different batches of pre-preg material were used. In each case of a new batch of material being used to make more specimens, a set of static tests were conducted to confirm the quasi-static strength. Figure 1 shows the three distinct failure modes obtained from the static tests as part of this study. The failure strengths are shown in table 2 for the multiple different batches and configurations tested along with the original data from [15].

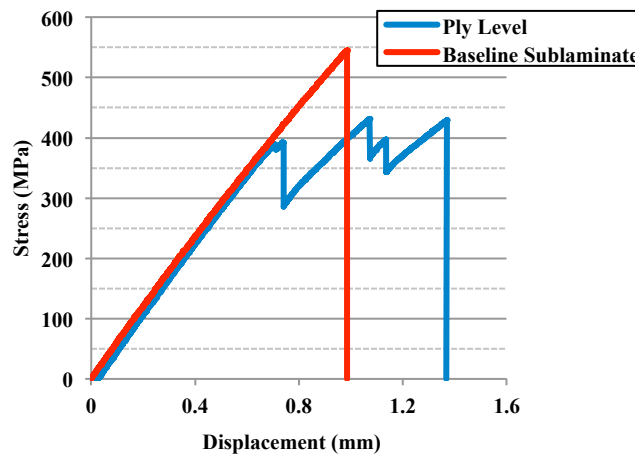


**Figure 1. Showing the three distinct failure modes after static tensile failure. (a) Pull-out from a baseline sub-laminate case, (b) Delamination from a ply-level case, and (c) brittle failure from a second sub-laminate case.**

**Table 2 Summary of the failure modes and strengths for each configuration and batch.**

Layup	Number of Specimens	Batch	Strength (MPa)	CV (%)	Failure Mode
Ply-level	5	1	418	6.6	Delamination
Ply-level	3	2	447	3.1	Delamination
Ply-level	4	3	396	5.4	Delamination
Ply-level	6	Original	396	5.2	Delamination
Sub-laminate	5	1	581	2.9	Pull-out
Sub-laminate	4	2	532	3.1	Pull-out
Sub-laminate	6	Original	500	3.95	Pull-out
Second Sub-laminate	3	1	475	4.8	Brittle
Second Sub-laminate	6	Original	433	2.0	Brittle

The first batches for the ply and baseline sub-laminate-level specimens used 5 specimens, and any batches thereafter including the second sub-laminate configuration used fewer specimens as the failure modes and strengths were already well documented.



**Figure 2. Typical load-displacement curves for a baseline sub-laminate level  $[45/90/-45/0]_{2S}$  test and a ply-level test  $[45_2/90_2/-45_2/0_2]_S$  with a hole diameter 3.175 mm.**

Load curves for the ply and baseline sub-laminate cases are shown in figure 2. Interrupted tests of these two cases at 80% of the static failure load for ply level and 85% for the baseline sub-laminate level tests respectively show typical damage levels from CT scans in figures 3 and 4. Despite the differences in the failure strength and overall failure mode, the sub-critical damage mechanisms are broadly similar for both configurations. Generally,

the first signs of damage observed in the laminate was matrix splitting in the surface +45° plies, propagating from the hole edge roughly where the fibre direction was tangential to the hole boundary. This was followed by isolated matrix splits in the 90° and -45° plies. For the ply-level case the damage was more localised to the hole-edge whereas for the baseline sub-laminate case the damage tended to be more distributed throughout the laminate. This is more noticeable for the matrix splitting of the 90° ply orientations.

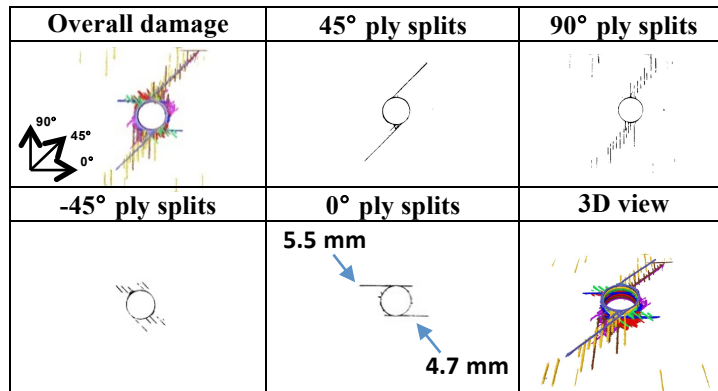


Figure 3. X-ray CT scan images from a ply-level  $[45_2/90_2/-45_2/0_2]_S$  test interrupted at 80% static load, showing the damage initiation (from top left), the global damage pattern, +45 splits, 90 splits, -45 splits and zero splits.

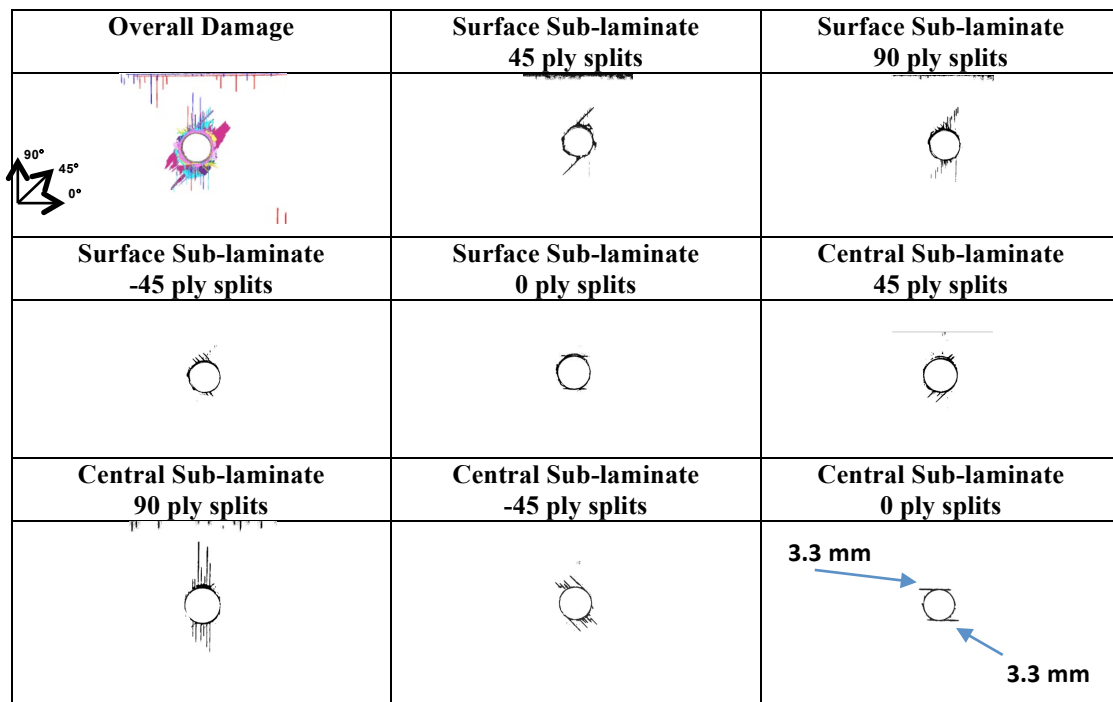


Figure 4. X-ray CT scan images from a baseline sub-laminate  $[45/90/-45/0]_{2S}$  level test with hole diameter 3.175 mm, interrupted at 85% static load, showing the damage initiation (from top left), the global damage pattern, +45 splits, 90 splits, -45 splits and zero splits.

## 4 Fatigue Testing

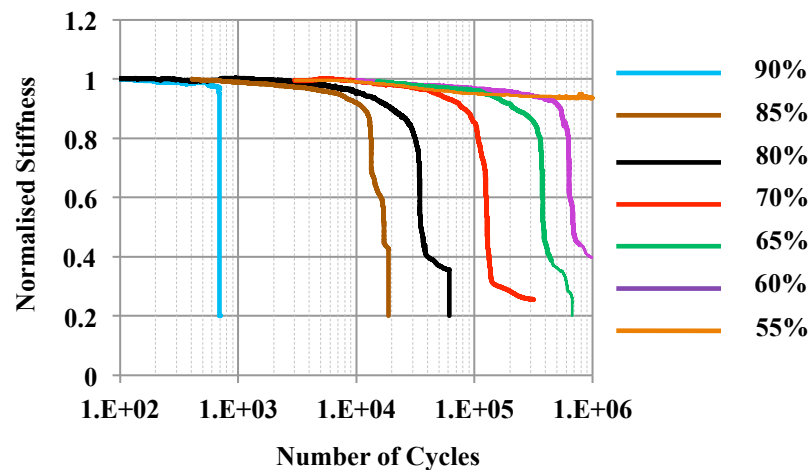
Following on from the quasi-static testing programme, the fatigue testing was carried out using the severities described in section 2. Figure 5 shows the loss in stiffness as damage develops for typical examples from the baseline sub-laminate case which can be compared to the ply level case from [19]. The normalised stiffness ( $E'/E'_0$ ) is plotted as a function of number of cycles where  $E'$  and  $E'_0$  is the residual and initial stiffness respectively. The effective cross sectional area carrying load, changes with increasing damage in the specimens due to delaminated plies becoming detached, thus causing the apparent loss in stiffness.

For the baseline sub-laminate specimens, fatigue failure appeared to follow a very similar trend to that of the ply level specimens with delamination dominating in all but the very highest severities (>90%). It is notable that this differed significantly from the quasi-static failure which was dominated by fibre failure (pull-out) with major delamination not progressing along the length of the specimen. It can thus be seen how the role of delamination is critical in the case of fatigue loading, even when it does not dominate in static tests. The significant loss of stiffness that relates to the accumulation of damage is characterised through interrupted testing, which is described in the next section.

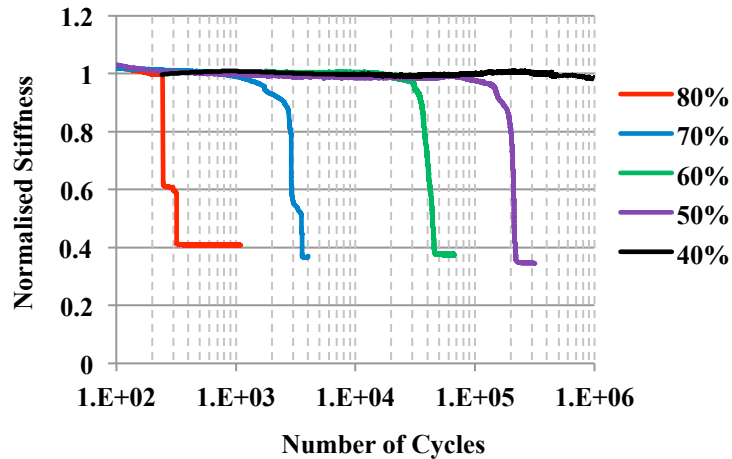
At the lower peak amplitudes the fibre-failure stresses are not reached during the development of damage prior to delamination across the full width of specimens. This gives delaminations the opportunity to propagate beyond the full width of the specimens at the 45/90 and 90/-45 interfaces to the -45/0 interface where the delamination extends throughout the gauge length. At 90% severity the fibre failure stress is reached during the propagation of the delamination from the hole to specimen edge and so causes a pull-out failure. This is primarily due to the load redistribution caused by the delamination failure causing a quasi-static failure of the zero degree plies and is not considered to be a fatigue failure of the fibres themselves. At fatigue severities lower than 85%, the stresses which cause fibre-failure can no longer be reached prior to the delaminations propagating back to the grips, causing the stiffness loss greater than 15% which is considered as failure. For those specimens tested at 85% severity three failed by pull-out failure, and four by delamination, suggesting a threshold between the two failure mechanisms.

In some cases fibre failure does still occur at lower severities, but only after complete delamination of all the interfaces to the point where only the fibres of the 0° plies are carrying the load. This is evident from the sharp drop in the stiffness as it begins to level out in the lower parts of the curve (figure 5). The ply-level specimens do not exhibit fibre failure even after complete delamination of the specimens therefore the stiffness levels out giving a continuous second plateau (figure 6).

In all severities lower than 90% for the baseline sub-laminate case, subcritical damage is mainly confined to the outer sub-laminate down to a normalised effective modulus of around 0.6 (figure 5). Then in the latter part of the stiffness drop the damage crosses over into the inner sub-laminate regions, this can be shown as a kink in the stiffness curves (e.g. 85% severity curve in figure 5). In the baseline sub-laminate layout (figure 5), the stiffness loss from the initial stiffness plateau is more gradual than the ply-level layout (figure 6) due to a more progressive sequence of damage events. The damage in general tends to be more dispersed throughout the laminate for the sub-laminate configurations. In contrast, in figure 6, the stiffness loss for ply-level specimens is more abrupt due to a more defined sequence of damage events which tends to be more localised around the hole. In the ply level experiments the maximum surface temperature was shown to be insignificant compared to the  $T_g$  of the material but increased with increasing damage throughout the duration of the decrease in stiffness [19].



**Figure 5. Typical fatigue stiffness curves at each severity for the baseline sub-laminate [45/90/-45/0]<sub>2s</sub> level test program with hole diameter of 3.175 mm.**



**Figure 6. Typical fatigue stiffness curves at each severity for the ply-level  $[45_2/90_2/-45_2/0_2]_S$  test program with hole diameter of 3.175 mm [19].**

Using the failure criterion of 15% reduction in normalised stiffness, an SN curve can be plotted, as in figure 7. The failure criterion is chosen as it represents the point by which an almost vertical slope is reached in the stiffness curves for all specimens. Each of the curves in figures 5 and 6 represents a test from the mid-range of the scatter seen in the S-N curve in figure 7. The transition from pull-out to delamination explains the high scatter at 85% severity for the baseline sub-laminate case, with early failures being pull-out and later failures being delamination. The 90% severity pull-out failures also shift the SN curve to the left, as pull-out failure occurs before delamination in the overall damage development sequence. When fitting all of the data values with a trend line, an  $R^2$  value of 0.865 is obtained. If the two failure modes are considered separately and only specimens that failed by delamination used, then a better fit to the trend line is obtained, with an  $R^2$  of 0.875. The damage progression in the baseline sublaminates is slower than for ply-level specimens due to the dispersed nature of the  $0^\circ$  plies, which hinders the delamination progression towards the inner sublaminates. When going from the ply-level configuration to baseline sublaminates level specimens the effective ply thickness is reduced and hence the ply thickness to hole diameter ratio is lower. For a smaller ply thickness to hole-diameter ratio the propensity for delaminations to propagate is reduced. This explains the notable differences between the two SN curves.

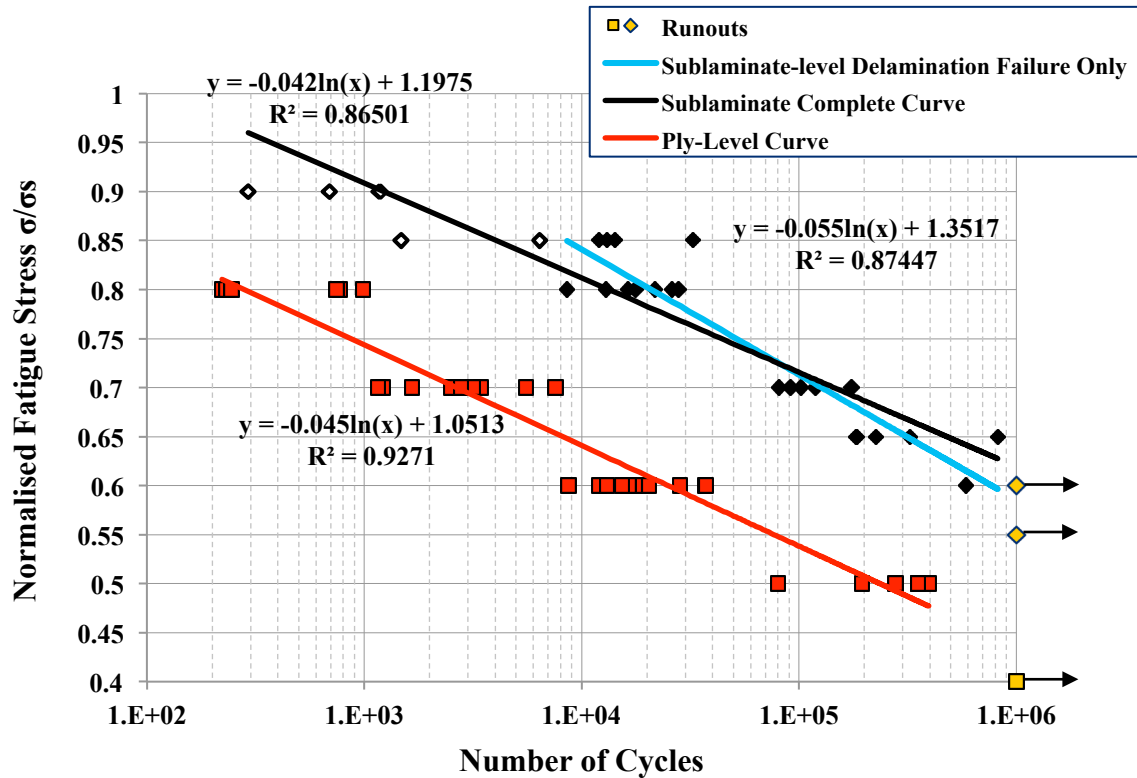


Figure 7. Plot showing both ply-level  $[45_2/90_2/-45_2/0_2]_s$  and baseline sub-laminate  $[45/90/-45/0]_{2s}$  SN curves for hole diameter of 3.175 mm, pull-out failures are indicated by the hollow diamond symbols (run-outs indicated using arrows).

Specimens from the second sub-laminate configuration were tested at 90, 85, 80 and 75% severity, where all severities consistently gave run-outs to  $1 \times 10^6$  cycles with very little stiffness loss even for the highest of severities tested. The level of damage at run-out and residual strength is discussed in section 6.3.

## 5. Fatigue Interrupted Testing and Damage Characterisation

As well as the specimens taken to full failure, several fatigue tests were interrupted during the stiffness loss/damage accumulation process. This process was extensively reported for the ply-level specimens in [19] and is compared and contrasted here with the baseline sub-laminate level tests. Since there was no stiffness loss for the second sub-laminate level specimens, the damage level was only assessed for run-out specimens, described in section 6.



In the 60% severity ply level test shown in figure 8 there is clear evidence of the delamination propagating at the -45/0 interface. Figure 8a shows the CT images, whilst 8b shows the planar delamination areas at each interface through the thickness, which indicates that the -45/0 interface is primarily responsible for the stiffness decrease. No delamination at this interface was observed in the static interrupted test at 80% of static load [19]. This is the most dominant damage process responsible for the sudden drop in the load in static failure and therefore is not observed until catastrophic failure, which in fatigue is more of a gradual process. All forms of damage initiate from the hole-edge.

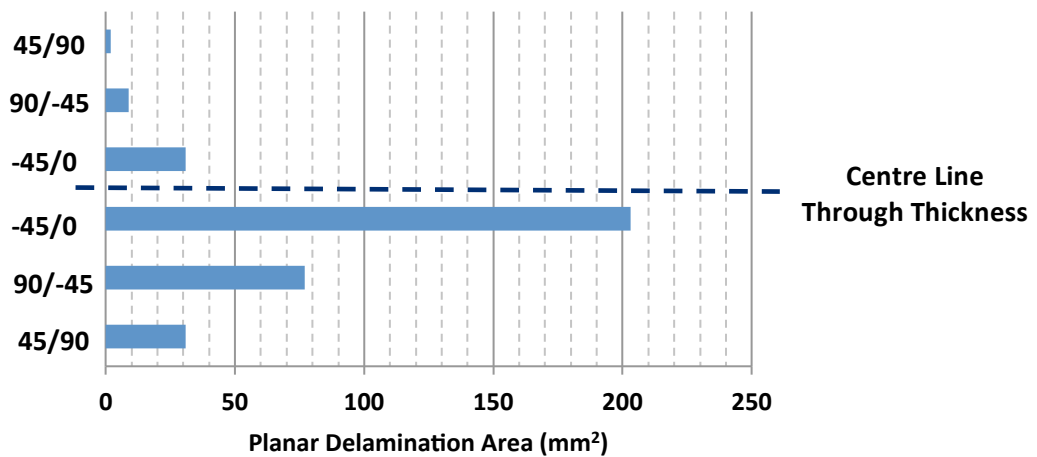
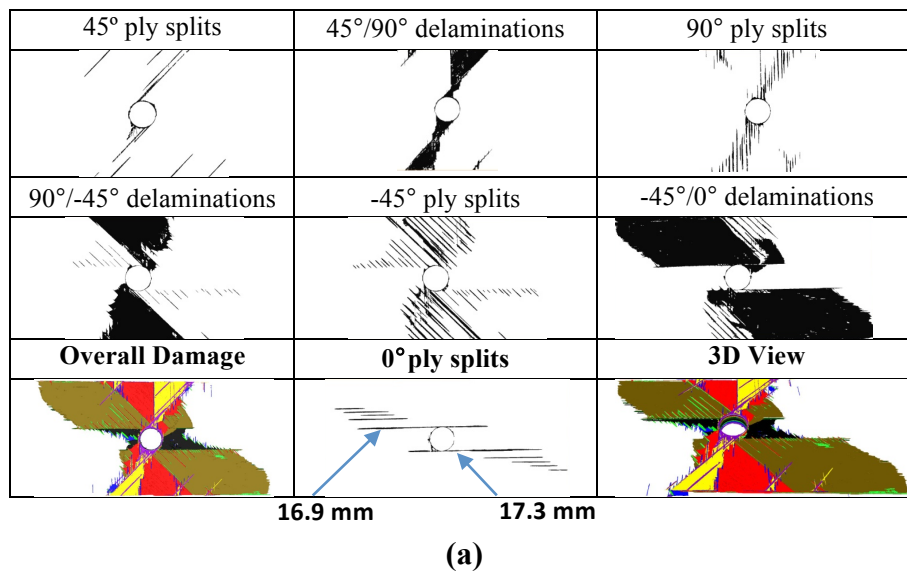
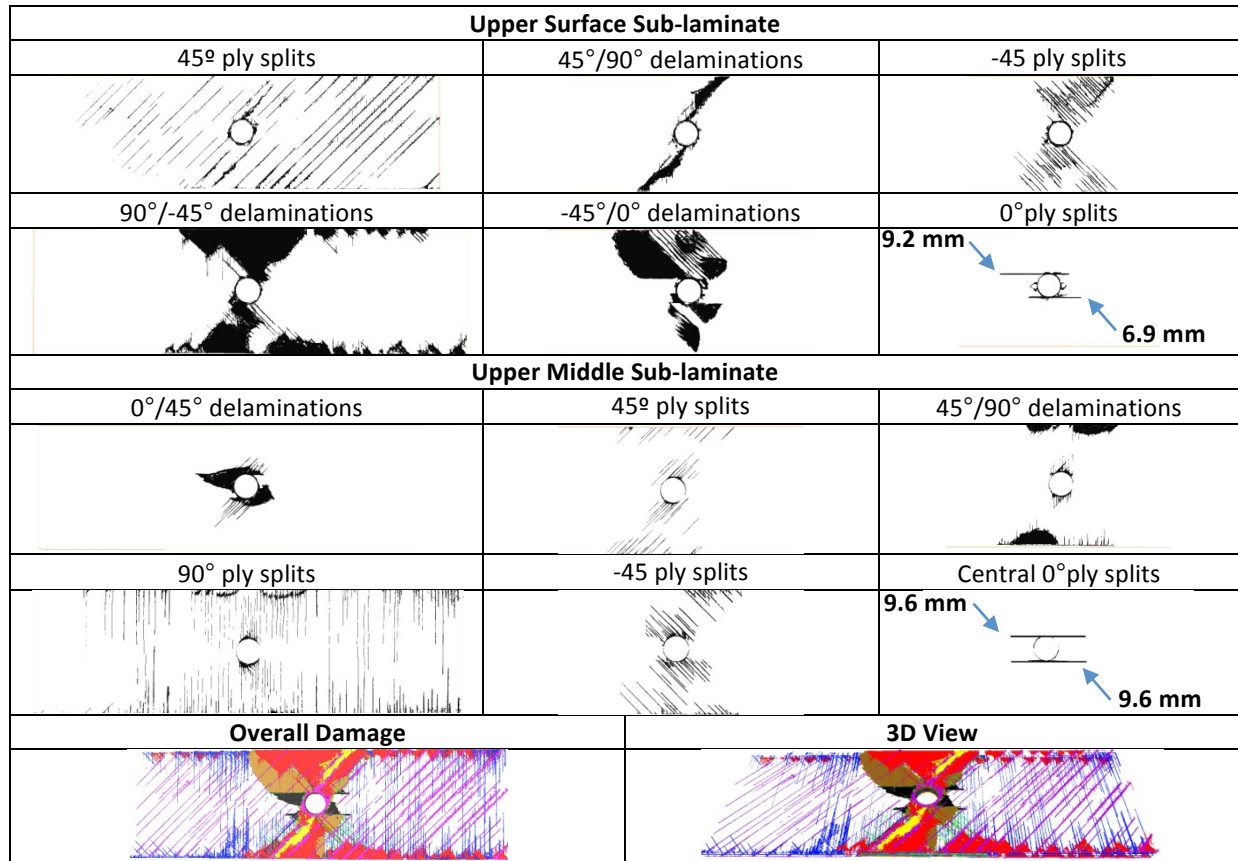


Figure 8. An interrupted test of a ply-level laminate  $[45_2/90_2/-45_2/0_2]_S$  at 60% severity with a stiffness loss of 15% (a) X-ray CT images [19], and (b) Bar graph quantifying delamination areas for each interface.

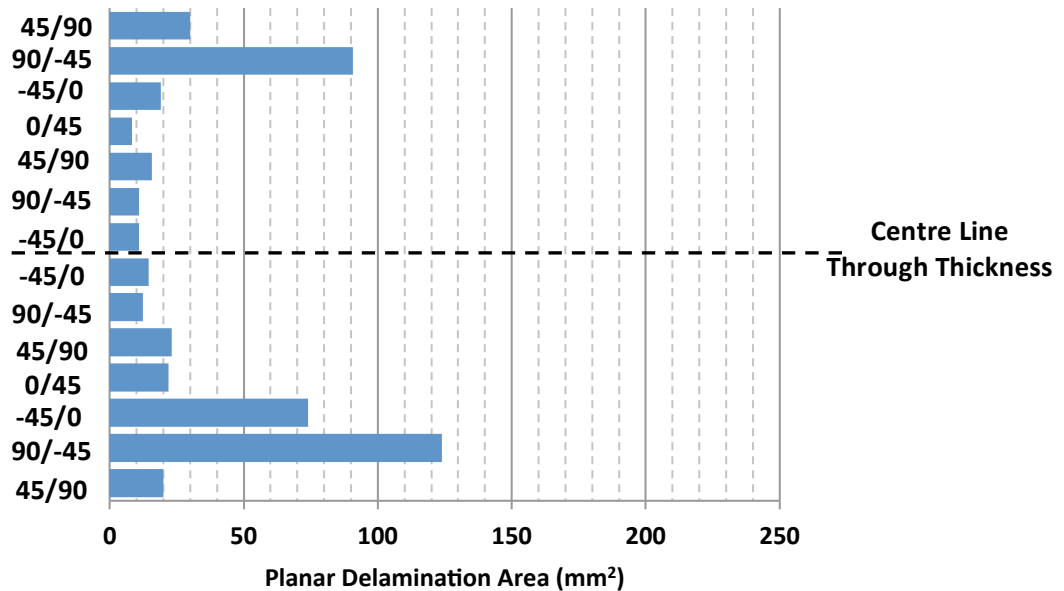
Two examples of baseline sub-laminate level fatigue tests at 80% severity are shown in figures 9 and 10, interrupted at 7% and 15% loss in stiffness respectively. There is extensive delamination at the surface -45/0 interface and also in between the long zero splits at the lower 0° interface to the +45 ply. This occurs relatively early in the drop in stiffness.

The 1<sup>st</sup> asymmetric delamination of the -45/0 interface occurs at 7% loss in stiffness (figure 9), which is followed by the propagation of the 2<sup>nd</sup> asymmetric delamination observed in figure 10 (15% stiffness loss). The second asymmetric -45/0 delamination ‘catches up’ with the 1<sup>st</sup> in terms of length at this point. The four delamination fronts then both propagate outwards towards the end tabs simultaneously. This is different to what was observed in ply-level, where a complete delamination of the 1<sup>st</sup> asymmetric -45/0 interface usually occurs prior to the propagation of the second, giving rise to the kinks in the stiffness loss curves.

The -45/0 delamination eventually crosses over into the areas between the zero splits at the next interface into the laminate (0/45) in the most severely damaged interrupted tests. This can be seen by the measurable delamination area at 0/45 on the horizontal bar charts of figures 9b and 10b. Also the matrix cracks are more dispersed in the surface plies and in the 90° plies throughout the laminate, with a significant level of edge delamination present at the inner sub-laminates. All of the splits and cracks are accompanied by small local delaminations at the adjacent interfaces and have a similar size to the ply thickness. Generally there is a significant amount of free-edge delamination in comparison to the ply-level interrupted tests. The delaminations initiate from the edges in the inner sub-laminates at the +45/90 and 90/-45 interfaces whereas for the surface +45/90 interfaces the delamination initiates from the hole-edges. This is due to the inner plies being more constrained. On reaching 15% loss in the stiffness, the edge delaminations have propagated further inwards towards the hole.

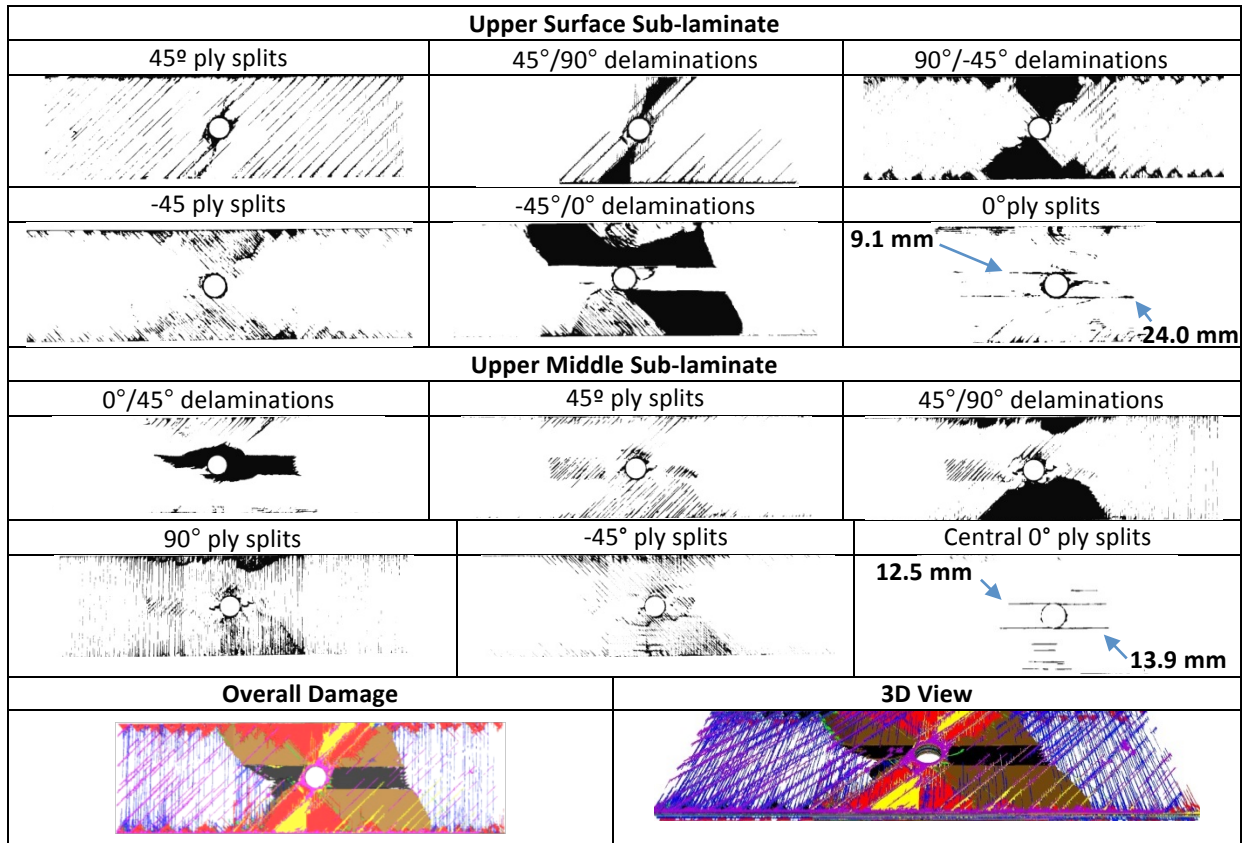


(a)

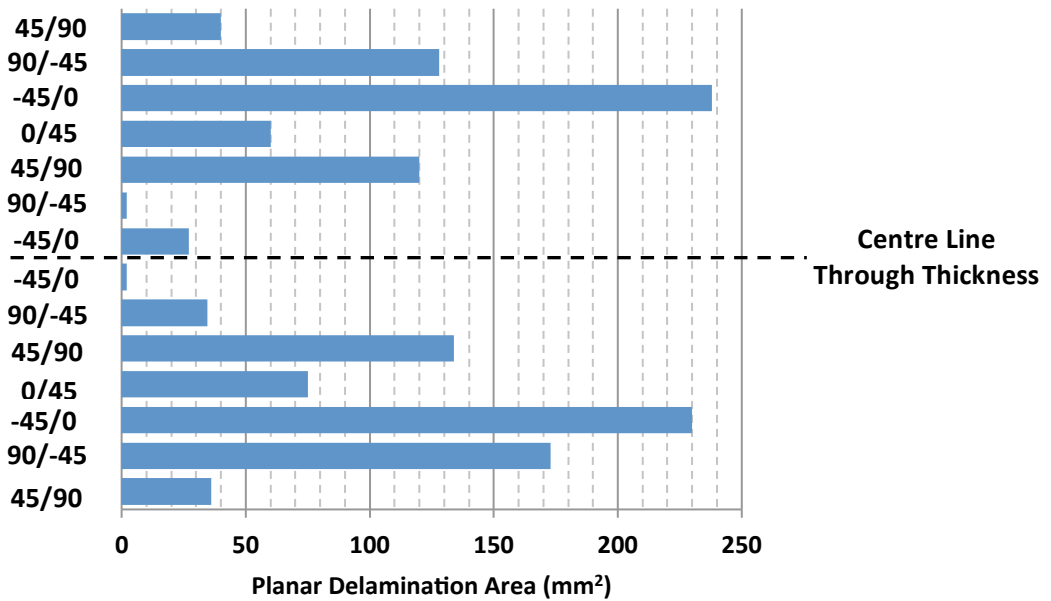


(b)

Figure 9. A baseline sub-laminate [45/90/-45/0]<sub>2S</sub> interrupted test at 80% severity with a stiffness loss of 7% (a) X-Ray CT Images and (b) Bar graph quantifying delamination areas for each interface.



(a)



(b)

Figure 10. A baseline sub-laminate[45/90/-45/0]<sub>2s</sub> interrupted test at 80% severity with a stiffness loss of 15% (a) X-Ray CT Images and (b) Bar graph quantifying delamination areas for each interface.

## 6. Residual Strength Testing

The ply level, baseline sub-laminate and second sub-laminate specimens that reached run-out were tested for residual strengths. One specimen from each configuration was used for X-ray CT analysis.

### 6.1 Ply-level Configuration

The ply level specimens gave consistent run-outs at 40% fatigue severity [19]. These were not tested for residual strength or presented in detail in [19] and so are shown here for comparison with the sub-laminate configurations. The X-ray CT image in figure 11 shows the damage for the ply-level configuration at 40% after  $1 \times 10^6$  cycles. There is relatively little damage, mainly splitting of the surface plies and matrix cracking of the  $90^\circ$  plies adjacent to the split. There is also some matrix cracking in the  $-45^\circ$  directions and some small splits in the  $0^\circ$  direction. There are no delaminations present after  $1 \times 10^6$  cycles at 40% except for some small delaminations at the bottom face due to drilling damage. All damage is local to the hole. The average residual strength for the five ply level specimens tested to run-out at 40% severity, was 403 MPa with a coefficient of variation of 4.89% (versus 396 MPa for virgin specimens from the same batch, see table 3). There is thus no notable change in the residual strengths over the unfatigued specimens due to the clear lack of fatigue damage (figure 11). There is also an absence of any notch blunting mechanism since the residual strength failure mode (delamination) is the same as that of fatigue. No increase in residual notched strength occurs in the ply-level case since it fails by delamination. Only specimens which are prone to fibre-dominated failures are affected by the notch blunting effect of the zero degree ply splits tangential to the hole where the reduction in stress concentration affects the failure of these load bearing zero degree plies, which are the main load bearing ones. Therefore in the ply-level case any fatigue damage simply contributes to the final quasi-static delamination failure, instead of retarding it as is seen in the fibre dominated residual strength tests below.

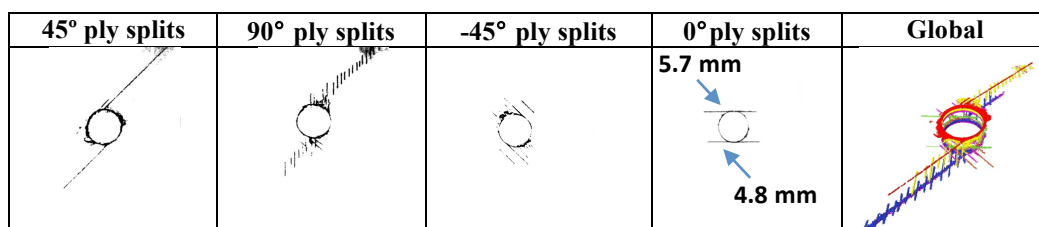


Figure 11. Typical ply level  $[45_2/90_2/-45_2/0_2]_S$  specimen with hole diameter of 3.175 mm, +45, 90, -45 and 0 degree splits after  $1 \times 10^6$  cycles at 40% severity prior to static residual strength test.

## 6.2 Baseline Sub-laminate Level Configuration

The baseline sub-laminate level specimens gave consistent run-outs at 55% fatigue severity. The residual tensile strength of these laminates showed a distinct increase following fatigue loading to  $1 \times 10^6$  cycles over the quasi-static result. The average static residual strength was 563 MPa for three specimens with a coefficient of variation of 0.4% (versus 531 MPa for the virgin specimens from the same batch, see table 3). The post run-out failure mode was pull-out, the same as the unfatigued specimens. Figure 12 shows the X-ray CT images of damage in a typical run-out specimen for a baseline sub-laminate level laminate at 55% severity after  $1 \times 10^6$  cycles.

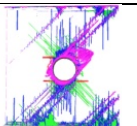
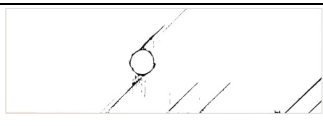
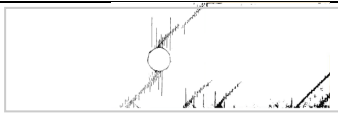

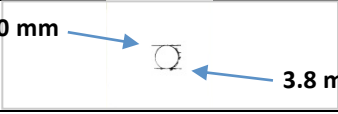
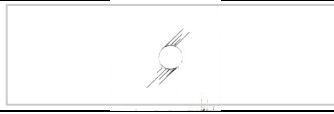
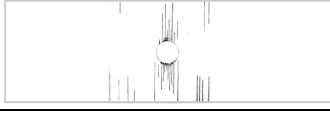
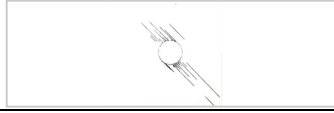
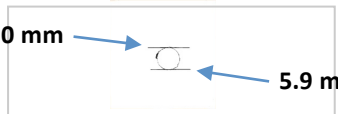
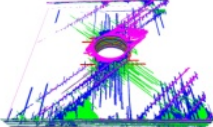
<b>Overall Damage</b>	<b>Surface Sub-laminate 45° Matrix Cracks</b>
	
<b>Surface Sub-laminate 90° Matrix Cracks</b>	<b>Surface Sub-laminate -45° Matrix Cracks</b>
	
<b>Surface Sub-laminate 0° Matrix Cracks</b>	<b>Central Sub-laminate 45° ply splits</b>
	
<b>Central Sub-laminate 90° ply splits</b>	<b>Central Sub-laminate -45° ply splits</b>
	
<b>Central Sub-laminate 0° Matrix Cracks</b>	<b>3D View</b>
	

Figure 12. X-ray CT slices for the baseline sub-laminate  $[45/90/-45/0]_{2S}$  level fatigue test at 55% severity.

The damage takes the form of matrix cracking in each of the ply orientations throughout the laminate. The damage is slightly more distributed than for the ply level specimen at 40%, but the majority of the damage still occurs around the vicinity of the hole. There were no obvious delaminations in any of the specimens that ran to  $1 \times 10^6$  cycles and therefore there is no apparent loss in the stiffness of the specimens as delamination damage accounts for the vast majority of the stiffness loss.

Increased post-fatigue residual strengths only occur in notched laminates which exhibit fibre-dominated failure. The  $0^\circ$  ply splits that occur during fatigue loading act to reduce the stress concentrations around the hole-edge and therefore delay the onset of fibre-failure.

For the sublaminated case if fatigue loading was carried out at a lower severity a runout would still be obtained, but with less splitting damage. Therefore the notch blunting effect would be reduced and residual strength would be closer to that of the unfatigued specimens.

### **6.3 Second Sub-laminate Configuration**

The second sub-laminate configuration gave consistent run-outs even at the highest of severities (90%) giving little or no loss of stiffness. Thus it does not satisfy the 15% stiffness loss failure criterion. Therefore the S-N curve in figure 10 shows only points from the first two layup configurations which reached the 15% stiffness loss failure criterion prior to runout at  $1 \times 10^6$  cycles. However the X-ray CT images in figures 13, 14 and 15 indicate significant matrix cracks and delaminations with different colours allocated to different damage modes and locations. In figures 13 and 14 the damage in purple corresponds to the  $45^\circ$  matrix cracks, green corresponds to delamination in the  $-45/90$  interface, red corresponds to  $-45^\circ$  cracks, and blue for the  $90^\circ$  cracks. The delaminations tend to occur in the outermost sub-laminates as can be seen in figure 19. As there are many more plies and interfaces than in the baseline sub-laminate case, this delamination doesn't contribute significantly to any observed loss in stiffness. Figure 14 shows the damage at 85% severity, likewise there are some delaminations in the outer plies, however the level of damage is significantly less than for 90% given that there is only a minor difference in the severity. At 75% severity only matrix splitting is observed in the specimen with no damage in the form of delaminations (figure 13).

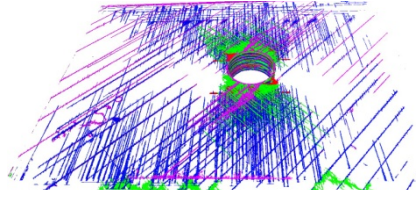


Figure 13. Overall damage for a second sublaminate  $[45/90/-45/0]_{4S}$  test at 75% severity after  $1 \times 10^6$  cycles.

Global Damage Plan View	Surface Sub-laminate 45 splits	Surface Sub-laminate -45/90 delamination
Surface Sub-laminate 0 Splits	Center Sub-laminate +45 Splits	Center Sub-laminate 90 Splits
Center Sub-laminate -45 Splits	Center Sub-laminate 0 Splits	3D View

Figure 14. X-ray CT slices for a second sub-laminate  $[45/90/-45/0]_{4S}$  level fatigue test at 85% severity.

Figure 15 shows a different colour scheme due to the extent of the different delamination planes. The 45/90 interface is light blue, -45/90 is shown in green, -45/0 is shown in red, the 0 splits are in dark green. Some of the edge delaminations are shown in yellow. Determination of exact damage planes proved difficult due to the number of plies and the overall ply thickness.



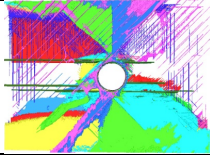




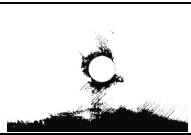
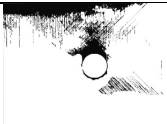


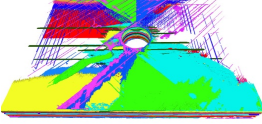
Global Damage Plan View	Surface Sub-laminate +45 Splits	Surface Sub-laminate +45/90 Interface
		
Surface Sub-laminate 90/-45 Interface	Surface Sub-laminate -45/0 Interface	Center Sub-laminate +45/90 Interface
		
Center Sub-laminate 90/-45 interface	Center Sub-laminate 0 Splits	Bottom Surface Sub-laminate -45/0 Interface
		
	Overall Damage	
		

Figure 15. X-ray CT slices for a second sub-laminate  $[45/90/-45/0]_{4S}$  level fatigue test at 90% severity.

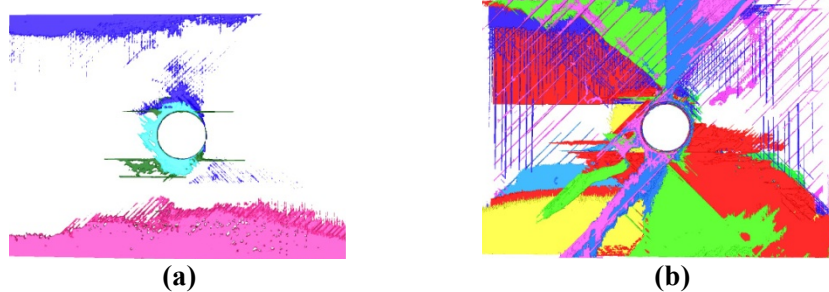
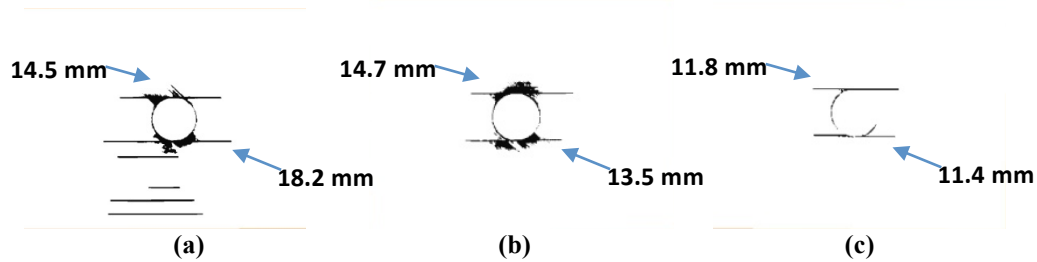


Figure 16. X-ray CT slices for the second sub-laminate  $[45/90/-45/0]_{4S}$  level fatigue test at 90% severity with (a) outer plies blanked and (b) inner plies blanked.

Tests were carried out for residual strength, using three specimens for each of 90% and 85% severity run-outs. Static residual strengths at 85% severity were marginally greater than the original quasi static results (498 MPa (2.1% CV) vs 475 MPa), and similarly for 90% severity (499 MPa (3% CV) vs 475 MPa). One test was carried out at 75% severity showed a residual strength of 522 MPa.

It appears that the central  $0^\circ$  ply splits, which control the notch blunting effect, are fairly similar in length for each severity tested. The overall damage is not controlling the notch blunting effects thus explaining why the residual strengths are similar for each of the severities tested despite the obvious differences in the overall damage from the X-ray CT images. Figure 17 shows the extent of the splitting in the central  $0^\circ$  plies for 90, 85 and 75% post-fatigue. The propagation of  $0^\circ$  ply splits is largely caused by shear stresses. There are many combinations by which these splits can initiate as defined by Daken and Mar [24].



**Figure 17. The extent of matrix splitting for the centremost  $0^\circ$  ply splits of a second sublaminate  $[45/90/-45/0]_{4S}$  test for (a) 90%, (b) 85%, and (c) 75% severities.**

The failure mode changes from brittle when testing un-fatigued specimens in quasi-static loading, to pull-out after  $1 \times 10^6$  cycles as fatigue loading had caused sufficient damage in the outer sub-laminates prior to residual strength tests. For pull-out failure to occur, a certain level of delamination growth must be present prior to the plies in the  $0^\circ$  direction reaching the stresses required for fibre failure. The CT images and visual observation of the specimens after residual strength testing therefore supports the failure mode change. Table 3 summarises the post fatigue residual strengths.

**Table 3. Summary of the post-fatigue residual strengths for each configuration.**

Layup	Severity	Number of Specimens	Batch	Strength (MPa)	CV (%)	Failure Mode
Ply-level	Pristine	4	3	396	5.4	Delamination
	40%	5	3	403	4.9	Delamination
Sub-laminate	Pristine	4	2	532	3.13	Pull-out
	55%	4	2	563	0.4	Pull-out
Second Sub-laminate	Pristine		1	475	4.8	Brittle
	90%	3	1	498	3.0	Pull-out
	85%	3	1	499	2.1	Pull-out
	75%	1	1	522	N/a	Pull-out

## 7. Conclusions

Carbon fibre epoxy laminates of various configurations with a centrally drilled hole, were loaded quasi-statically and under fatigue. In quasi-static ply-level tests, extensive delaminations are observed at the point of failure. Under fatigue loading, the same delamination dominated mode of failure is also observed. For the quasi-static baseline sub-laminate level tests, a fibre dominated pull-out failure mode is observed, however in fatigue tests, a delamination dominated failure mode is observed in all but the highest of severities tested. Therefore for the baseline sub-laminate level tests, a different mode of failure is observed in fatigue tests to those of quasi-static tests. X-ray computed tomography (CT) data of the interrupted tests showed that, initially damage starts to propagate out from the hole edge in terms of matrix cracks and delamination. Asymmetric -45/0 delaminations cause a large drop in stiffness. This is the dominant failure event for both the ply level and sub-laminate level specimens. The failure events for the ply level specimens are more localised around the hole, giving a more abrupt decrease in stiffness from the initial plateau. For the baseline sub-laminate level specimens, damage occurs in the outer sub-laminates first and then passes through into the central sub-laminates with a greater degree of distributed matrix cracking. This gives rise to a more progressive damage sequence leading to failure.

Historically the de-ply technique was more commonly used in order to determine the extent of delaminations and their locations within the laminate. This method however is destructive due to the pyrolysis of the matrix resin. X-ray CT is becoming a more routine method which produces a 3D volume of the damage which can be segmented to reveal the precise locations within a laminate in a non-destructive fashion. X-ray CT also supersedes 2D X-radiography methods which produced images containing a superimposition of the overall damage in which precise damage locations cannot be identified. This paper therefore presents one of the first quantitative datasets which thoroughly assesses fatigue delamination via X-ray CT.

A third layup, with a sub-laminate configuration and specimen dimensions scaled up by a factor of 2 in the thickness, width, and hole diameter was tested. In previous studies this configuration was shown to give brittle failure in quasi-static loading. In fatigue loading this configuration gave run-outs with no measurable loss in stiffness for all severities tested, despite the presence of extensive delaminations in the highest severities. On further examination of the CT images at 85% and 90%, it was apparent that the delaminations were mostly

present in the outer sub-laminates so the fact that the initial stiffness is maintained to run-out can be attributed to the fact that a relatively small percentage of plies (which are not in the zero direction and so carry less load) are affected.

Run-out specimens for the different configurations were subjected to quasi-static loading to failure and for the fibre-dominated sub-laminate case showed an increase in static residual strength properties. The residual strength properties for the second sub-laminate configuration were shown to have only a slight increase on the quasi-static strengths. In this case, despite the varying levels of overall damage in each of the severities tested, the extent of splitting in the central 0° plies were found to be similar therefore the residual strengths were similar. The increase in the residual properties are therefore independent of the overall damage but highly dependent on the extent of the matrix splits of the central 0° plies, reducing the stress concentrations around the hole, thus delaying the onset of fibre-failure. It was found that the propagation of matrix splits of the central 0° plies generally followed the delamination front in the -45/0 interface.

## **Acknowledgements**

The authors would like to acknowledge the support of the Engineering and Physical Sciences Research Council (EPSRC) to the Advanced Composites Centre for Innovation and Science (ACCIS) Doctoral Training Centre (DTC), grant number EP/G036772/1.

## **References**

- [1] Spearing SM, Beaumont PWR, Kortschot MT. The fatigue damage mechanics of notched carbon-fiber PEEK laminates. *Composites*. 1992;23(5):305-11.
- [2] Broughton WR, Gower MRL, Lodeiro MJ, Pilkington GD, Shaw RM. An experimental assessment of open-hole tension-tension fatigue behaviour of a GFRP laminate. *Composites Part a-Applied Science and Manufacturing*. 2011;42(10):1310-20.
- [3] Kawai M, Shiratsuchi T. Vanishing notch sensitivity approach to fatigue life prediction of notched cross-ply CFRP laminates at room temperature. *Journal of Composite Materials* 2012;46(23):2935-50

- [4] Mohlin T, Carlsson L, Blom AF. An X-ray radiography study of delamination growth in notched carbon/epoxy laminates. Proc Conf Testing, Evaluation and Quality Control of Composites. Guildford, England: Butterworths; 1983. p. 85-92.
- [5] Mohlin T, Blom AF, Carlsson L, Gustavsson AI. Delamination growth in notched graphite/epoxy laminates under compression fatigue loading. ASTM STP 876. 1985;Delamination and Debonding of Materials, W. S. Johnson (ed.):168-88.
- [6] Scott AE, Mavrogordato M, Wright P, Sinclair I, Spearing SM. In situ fibre fracture measurement in carbon-epoxy laminates using high resolution computed tomography. Composites Science and Technology. 2011;71(12):1471-7.
- [7] Moffat AJ, Wright P, Buffiere JY, Sinclair I, Spearing SM. Micromechanisms of damage in 0 degrees splits in a [90/0](s) composite material using synchrotron radiation computed tomography. Scripta Materialia. 2008;59(10):1043-6.
- [8] Bakis CE, Simonds RA, Vick LW, Stinchcombe WW. Matrix toughness, long term behaviour, and damage tolerance of notched graphite fiber-reinforced composite materials. In: Garbo SP, editor. Composite materials: testing and design, 9th ed. ASTM STP 1059. 1990:349-70.
- [9] Bakis CE, Yih HR, Stinchcombe WW, Reifsnider KL. Damage initiation and growth in notched laminates under reversed cyclic loading. In: Lagace PA, editor. Composite materials: fatigue and fracture, ASTM STP 1012 1989:66-83.
- [10] Simonds RA, Bakis CE, Stinchcombe WW. Effects of matrix toughness on fatigue response of graphite fiber composite laminates. In Legace PA, editor. Composite materials fatigue and fracture, 2nd ed. ASTM STP 1012. 1989:5-18.
- [11] Simonds RA, Stinchcombe WW. Response of notched AS4/PEEK laminates to tension-compression loading. In: Newaz GM, editor. Advances in thermoplastic matrix composite materials, ASTM STP 1044. 1989:133-45.
- [12] Ambu R, Aymerich F, Bertolino F. Investigation of the effect of damage on the strength of notched composite laminates by digital image correlation. The Journal of Strain Analysis for Engineering Design. 2005;40(5):451-61.

- [13] Spearing SM, Beaumont PWR. Fatigue damage mechanics of composite-materials 1. Experimental-measurement of damage and post-fatigue properties. *Composites Science and Technology*. 1992;44(2):159-68.
- [14] Wang CM, Shin CS. Residual properties of notched [0/90]4S AS4/PEEK composite laminates after fatigue and re-consolidation. *Composites Part B: Engineering*. 2002;33(1):67-76.
- [15] Green BG, Wisnom MR, Hallett SR. An experimental investigation into the tensile strength scaling of notched composites. *Composites Part a-Applied Science and Manufacturing*. 2007;38(3):867-78.
- [16] Nixon-Pearson O.J., Hallett. SR. An investigation into the damage development and residual strengths of open-hole specimens in fatigue. *International Conference on Composite Materials*. Montreal2013.
- [17] Nixon-Pearson OJ, McCombe GP, Hallett SR. An investigation into the damage development of open-hole specimens in fatigue. *European Conference on Composite Materials*. Venice2012.
- [18] Nixon-Pearson OJ, Hallett SR, Harper PW, Kawashita LF. Damage development in open-hole composite specimens in fatigue. Part 2: Numerical modelling. *Composite Structures*. 2013;106(December):890-8.
- [19] Nixon-Pearson OJ, Hallett SR, Withers PJ, Rouse J. Damage development in open-hole composite specimens in fatigue. Part 1: Experimental investigation. *Composite Structures*. 2013;106(December):882-9.
- [20] Hexcel 8552, Epoxy Matrix Product Datasheet. pdf download from:  
[www.hexcelcomposites.com/Markets/Products/Prepreg/PrepregDownld.html](http://www.hexcelcomposites.com/Markets/Products/Prepreg/PrepregDownld.html).
- [21] Withers PJ, Preuss M. Fatigue and Damage in Structural Materials Studied by X-Ray Tomography. *Annu Rev Mater Res*. 2012;42:81-103.
- [22] Hallett SR, Green, B.G., Jiang, W.G., and Wisnom, M.R. An Experimental and numerical investigation into the damage mechanisms in notched composites. *Composites Part A*. 2009;40(5):613-24.
- [23] Wright P, Moffat A, Sinclair I, Spearing SM. High resolution tomographic imaging and modelling of notch tip damage in a laminated composite. *Composites Science and Technology*. 2010;70(10):1444-52.
- [24] Daken HH, Mar JW. Splitting initiation and propagation in notched unidirectional graphite/epoxy composites under tension-tension cyclic loading. *Composite Structures*. 1985;4(2):111-33.